https://doi.org/10.30758/0555-2648-2021-67-2-177-207
УДК 523.98 550.388 551.5



ОБЗОР REVIEW

# INFLUENCE OF COSMIC WEATHER ON THE EARTH'S ATMOSPHERE

*OLEG A. TROSHICHEV[1*], IRINA P. GABIS[1], ALEXEI A. KRIVOLUTSKY[2]*

[1] — *State Scientific Center of the Russian Federation Arctic and Antarctic Research Institute, St. Petersburg, Russia*

[2] — *Federal State Budgetary Institution «Central Aerological Observatory», Moscow, Russia*

[*]*olegtro@aari.ru*

**Summary**

The review generalizes experimental data on the relationships between the solar activity agents (space weather) and atmosphere constituents. It is shown that high-energy solar protons (SPE) make a powerful impact on photo-chemical processes in the polar areas and, correspondingly, on atmospheric circulation and planetary cloudiness. Variations of the solar UV irradiance modulate the descent rate of the zonal wind in the equatorial stratosphere in the course of quasi-biennial oscillation (QBO), and thus control the total duration (period) of the QBO cycle and, correspondingly, the seasonal ozone depletion in the Antarctic. The geo-effective solar wind impacts on the atmospheric wind system in the entire Southern Polar region, and influences the dynamics of the Southern Oscillation (ENSO).

**Keywords**: atmospheric circulation, Earth's atmosphere, geoeffective solar wind, high-energy solar protons (SPE), model computations, ozone depletion, planetary cloudiness, quasi-biennial oscillation (QBO), solar UV irradiance, Southern Oscillation (ENSO), Space weather.

**For Citation:** *Troshichev O.A., Gabis I.P., Krivolutsky A.A.* Influence of cosmic weather on the Earth's atmosphere. *Problemy Arktiki i Antarktiki.* Arctic and Antarctic Research. 2021, 67 (2): 177–207. https://doi.org/10.30758/0555-2648-2021-67-2-177-207.

**Received 22.03.2021** **Revised 04.06.2021** **Accepted 05.06.2021**

# ВЛИЯНИЕ КОСМИЧЕСКОЙ ПОГОДЫ НА ЗЕМНУЮ АТМОСФЕРУ

*О.А. ТРОШИЧЕВ[1*], И.П. ГАБИС[1], А.А. КРИВОЛУЦКИЙ[2]*

[1] — *ГНЦ РФ Арктический и антарктический научно-исследовательский институт, Санкт-Петербург, Россия*

[2] — *ФГБУ Центральная аэрологическая обсерватория, Долгопрудный, Московская область, Россия*

[*]*olegtro@aari.ru*

**Резюме**

В обзоре обобщены экспериментальные данные о влиянии космической погоды на земную атмосферу. Показано, что высокоэнергичные солнечные протоны (SPE) оказывают мощное воздействие на фотохимические процессы в полярных областях и, соответственно, на атмосферную циркуляцию и планетарную облачность. Вариации солнечного УФ-излучения моделируют скорость спуска зональных ветров в экваториальной стратосфере в ходе квазидвухлетней осцилляции (QBO) и контролируют, таким образом, общую продолжительность (период) QBO цикла и, соответственно, вариации общего содержания озона в Антарктике. Геоэффективный солнечный ветер воздействует на систему катабатических ветров во всей южной полярной области и влияет на динамику южной осцилляции (ENSO).

**Ключевые слова:** атмосфера Земли, атмосферная циркуляция, высокоэнергичные солнечные протоны, геоэффективный солнечный ветер, квазидвухлетняя осцилляция (QBO), космическая погода, модельные расчеты, озоновая «дыра», планетарная облачность, солнечное УФ-излучение, южная осцилляция (ENSO).

**Для цитирования:** *Troshichev O.A., Gabis I.P., Krivolutsky A.A.* Influence of cosmic weather on the Earth's atmosphere. Проблемы Арктики и Антарктики. 2021, 67 (2): 177–207. https://doi.org/10.30758/0555-2648-2021-67-2-177-207.

**Поступила 22.03.2021** **После переработки 04.06.2021** **Принята 05.06.2021**

## INTRODUCTION

The term "space weather" refers to a complex of phenomena and processes in the heliosphere determined by the solar activity. In the ordinary, narrower sense, the term applies to the space controlled by the Earth's magnetic field, i.e. to the Earth's magnetosphere. The concept of the solar activity includes a number of various electromagnetic and mass emissions, which are provided by the processes taking place permanently in the atmosphere and convective zone of the Sun. The main agents of the solar activity that influence the Earth's atmosphere are the solar UV irradiance, solar high-energy particles E < 500 eV (SEP) (or the solar cosmic rays — SCR), a permanent stream of the galactic cosmic rays E > 1 GeV (GCR) modified by the solar activity, high energy particles accelerated in the magnetosphere (auroral electrons), and the solar wind — low-energy solar plasma with the frozen magnetic field permanently ejected by the Sun.

The visible and the infrared solar irradiation provides the main input in the total solar irradiance (TSI), with the total energy absorption in the Earth's atmosphere $E = 1366$ W/m$^2$. TSI practically does not vary during the solar cycle (change < 0.1%), that is why the total irradiance has usually been called "solar constant". The input of the solar and galactic cosmic rays, high energy particles and solar wind in the total irradiance is negligible, and the existing models of the atmosphere variability do not take into consideration short-term changes of the solar activity. However, in contrast to the total solar irradiance, the energy input of cosmic rays and energy particles can increase hundreds and more times in the periods of high solar activity. These particles strongly ionize the atmosphere at different altitudes and the corresponding changes of different atmospheric constituents can lead to a crucial modification of the atmospheric processes.

The term "atmosphere" refers to a layer of gases that are held near the Earth, from the sea level up to the height of ~ 100 km, due to the gravitational force. The Earth's atmosphere is divided into four main regions, namely: *the troposphere* (from 0 to about 12 km) — the warmest layer near the Earth due to the heat rising from the Earth's surface, *the stratosphere* (12–50 km) — the layer with a large concentration of ozone gases, which absorb most of the solar UV irradiation, protecting the Earth

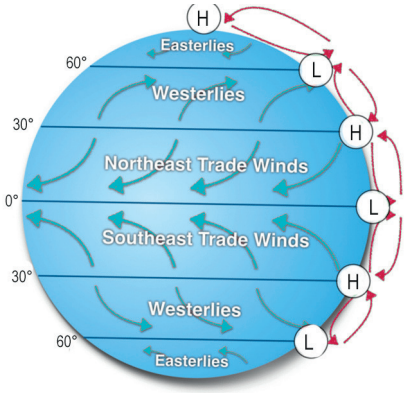


Fig. 1 Global system of atmospheric circulation, with the low pressure zones marked as L and the high pressure zones marked as H

Рис. 1. Глобальная система атмосферной циркуляции, где зоны низкого давления отмечены знаком L, а зоны высокого давления — знаком H

from harmful ultra violet (UV) rays, *the mesosphere* (50–80 km) — the coldest of the atmospheric regions, where the water vapours freeze and create clouds made purely of ice, and *the thermosphere* (80–500 km), including *the ionosphere*) – the layer where the temperatures can rapidly increase and decrease because of the thin air and proximity to the sun. The weather at the ground level is determined by short-term changes of such tropospheric parameters as temperature, humidity, air pressure, precipitation, and wind speed and direction.

Atmospheric processes such as radiation transfer, convection and aerosol movement play important roles in regulating the temperature and water cycles and protecting the mankind from excessive heat and the harmful radiation from the Sun. The atmospheric large-scale winds give rise to large and slow moving currents in the oceans. The oceans in turn provide an input of energy and water vapour into the air. The large-scale movement of air masses caused by the joint action of solar heating, the Earth's daily rotation and by the Coriolis force, was named atmospheric circulation. The idealised global circulation can be described as a world-wide system of winds which accomplish the transport of heat from the tropical to the polar latitudes (Figure 1). In each hemisphere there are three section (*Hadley cell*, *Ferrell cell* and *Polar cell*) where the air circulates through the entire depth of the troposphere. The land surface air masses in the *Hadley Cell* (at the latitudes from 0° to 30° N and S) flow towards the equator as easterlies; the circuit is closed by an air mass which lifts in the "equatorial low" zone, moves in the upper stratosphere to the latitude of ~ 30° N and S and lowers to the surface in this zone, named "the subtropical high". The warm surface air masses in the *Ferrell cell* (at the latitudes from 30° to 60° N and S) predominantly flow from the subtropical high as westerlies. At the polar latitudes the cold dense air sinks near the poles and blows towards the middle latitudes as the polar easterlies. Being strongly affected by the ocean currents and the surface orography, the real atmospheric circulation is dependent on the distribution of the continents and oceans and, as a result, is different in the northern and the southern hemispheres. Thus, the atmospheric circulation redistributes the thermal energy on the surface of the Earth and determines the Earth's climate.

The polar cells crucially respond to the solar heating and demonstrate strong seasonal changes (oscillations) dependent on the tilt of the Earth's rotation axis relative to the Sun (i.e. on the zenith angle of the Sun). As a result, the Arctic Oscillation (AO) and the Southern Oscillation (SO) are the dominant modes of the planetary climatic systems on the Earth. The Arctic Oscillation [1] is the mean-monthly sea level pressure variability over the Northern Hemisphere caused by the gradient of the sea level pressure between the Arctic basin and the middle latitudes. The North Atlantic Oscillation (NAO) has long been recognized as the major circulation pattern influencing the weather from the eastern North America to Europe. The amplitude of NAO is commonly characterized by the NAO index, which represents the normalized sea-level pressure difference between stations in the Azores and Iceland. The Southern Oscillation (SO) is determined as a negative correlation between the pressure fluctuations at the sea level in the Southeast Pacific high and the North Australian-Indonesian low. The anomalous warming of the surface water in the Eastern Pacific is named El Niño and the cold phase is named La Nina. This coupled system links El Niño to the atmospheric branch of SO and is named ENSO [2]. The Southern Oscillation is characterized by the SOI index, which is negative when ENSO is in a warm phase (El Niño events) and positive when ENSO is in a cold phase (La Nina events). The ENSO is the most pronounced year-to-year fluctuation of the climate system on the Earth, which strongly influences the other planetary climatic systems, including the NAO and AO. The effect of the statistically justified correlation between the NAO, ENSO and other circulation patterns and the variability of the climatic system in distant regions is termed "teleconnection". The phenomenon of teleconnection is derived from the fact that the stream from the WSSP (Western Subtropical South Pacific ) area with an extremely high temperature at the level of the ocean (SST anomaly) usually spreads in the South–East direction, forming the Antarctic Circumpolar Current (ACC) in the Southern ocean. This circumpolar current branches out northward into the Atlantic and Indian oceans with a strong impact on the weather conditions in these longitudinal sectors.

Thus, the global atmospheric circulation is divided into several climatic systems, whose characteristics can strongly change from year to year in spite of the fact that the total solar irradiation (TSI), the main factor of the solar influence on the Earth, practically does not vary during the solar cycle. The most dramatic alterations take place at high latitudes, suggesting that the polar vortices are significantly affected by the solar activity. This review presents experimental evidence of space weather influence on the Earth's atmosphere, with the main attention paid to the contribution made by research carried out in Russia. The following topics are examined: (1) Effect of energetic particles of the solar, galactic and magnetospheric origin, (2) Model computations of the cosmic rays influence on atmospheric processes, (3) Ozone depletion in the Antarctic and the solar UV irradiance, (4) The solar wind influence on atmospheric processes.

## 1. Influence of energetic particles on the Earth's atmosphere

### *1.1. Ionization produced by energetic particles (altitudinal profiles and ionization rates)*

Energetic particle precipitation (EPP) plays a significant role in many atmospheric processes [3, 4]. Various sources of ionization penetrate to different atmospheric levels and demonstrate different ionization rates. Figure 2 [4] demonstrates the efficiency of various ionizers as instantaneous ionization raters (in $cm^{-3}s^{-1}$) at different altitudes of penetration.

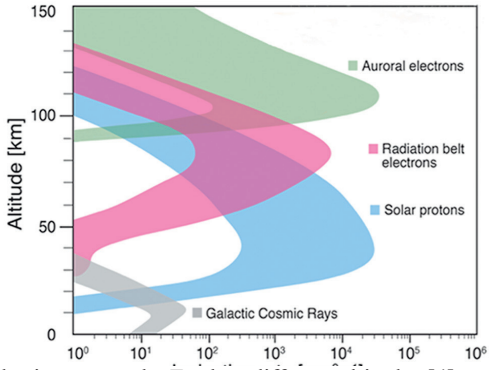


Fig. 2. Energetic particles impact on the Earth at different altitudes [4]

Рис. 2. Ионизация, производимая на разных высотах различными заряженными частицами [4]

High-energy particles of the galactic origin or galactic cosmic rays (GCR) consist mainly of protons with energy in the range from a few MeV to GeV [3]. They penetrate into the Earth's atmosphere down to the ground level and provide ionization rates up to 40 ion pairs ($cm^{-3}s^{-1}$) in the troposphere ($h \sim 10$ km). Maximum cosmic rays ionization rates are observed at the altitude 15–26 км, depending on the level of solar activity. The geomagnetic field acts as a shield for the incident cosmic rays and filters GCR particles according to their energy. The effect of geomagnetic shielding is characterized by a cut-off rigidity Rc: the lower the geomagnetic latitude, the higher is the rigidity, and the higher is the energy of GCR penetrating the atmosphere at this latitude. Particles with the energy E > 10 GeV can pass through the geomagnetic shield even in the equatorial area. The galactic cosmic rays are constantly present in the Earth's atmosphere, their intensity is modulated by the solar activity cycle: the higher the solar activity, the smaller the number of GCR events.

Solar energetic particles (SEP), mainly protons with energy in the range from tens keV to higher than100 MeV, are named the solar cosmic rays (SCR). They are related to solar eruptive areas or accelerated in the space [5]. The SEP events are sporadic phenomena, which are typical of epochs of maximum solar activity: the larger the SEP intensity, the less frequent is their occurrence. Solar protons penetrate down to the stratosphere ($h$ = 30–60 km) in the polar regions.

Solar wind serves as the main source of high-energy electrons, which are trapped and accelerated in the Earth's magnetosphere. The high-energy electrons, with energy from ~ 30 keV up to several MeV, emitted from the radiation belts (REP), produce ionization rates mostly in the mesosphere-thermosphere at heights of 60–100 km. The electrons with energy Ee = 1–100 keV (auroral electrons), originating in the external magnetosphere, produce ionization of > $10^4$ $cm^{-3}s^{-1}$ in the lower thermosphere ($h$ = 90–120 km). Their energy deposition is confined to the auroral oval. The auroral and radiation belt electron precipitations occur in connection with magnetospheric disturbances and reach maxima during the decay phase of the solar cycle. The magnetospheric-auroral electrons are absorbed in the upper atmosphere, but the bremsstrahlung produced by these electrons can penetrate down to 20 km [3, 4, 6].

Solar UV and X irradiations provide ionization rates ~$10^3$–$10^4$ ion pairs $cm^{-3}s^{-1}$ in the thermosphere, at altitudes about 100–150 km. The UV irradiation is responsible for the

generation of the ionospheric conductivity in high-latitude regions in the summer season. Solar UV irradiation in the range from 200 to 400 nm penetrates into the stratosphere and troposphere. Visible and infrared irradiation penetrates to the Earth's surface. The total solar irradiance changes over a wide range of periods, from minutes to the 11-year solar cycle. The irradiance of the Sun varies in phase with the solar cycle with an amplitude of ~ 0.1 % and a period of roughly 11 years. During the solar storm period in October 2003, the total solar irradiance (TSI) dropped by an unprecedented 0.34 % due to the dark large sunspots. Geomagnetic field restricts the intrusion of energetic particles in the low- and mid-latitudinal atmosphere according to their energy [3, 7, 8], but the high-latitudinal atmosphere is accessible to all types of particles, from the solar UV irradiation to the galactic cosmic rays.

### *1.2. Ionization processes affected by energetic particle precipitation*

The main chemical composition of the Earth's atmosphere is roughly the same from the ground level to 100 km, but physical conditions that are of primary importance in atmospheric dynamics and climate are essentially different at different altitudes and latitudes. For example, the temperature in the low and middle atmosphere is different by 100°K, and the atmospheric density is different by 6 orders of magnitude. The ionization rate in the atmosphere (which is mainly neutral) changes with space and time and brings into action various physico-chemical processes which can initiate processes in the atmosphere, from the global circulation to climatic changes.

If the primary particle has sufficient energy to enter the atmosphere, it accidentally collides with the nucleus of one of the atmospheric gases, where the most abundant nuclei are nitrogen (N) and oxygen (O). All energetic precipitating particles (EPP) ionize neutral molecules ($N_2$ or $O_2$) in the Earth's atmosphere and produce chemically active radicals such as N, NO, H, HO, which can be further transformed by gas phase chemistry. Additional amounts of $NO_X$ and $HO_X$ will intensify the process of ozone oxidation and, correspondingly, ozone depletion. The effects of the short-lived radicals $HO_X$ are localized in space and time: they are observed only where particle precipitation occurs. The radicals $NO_X$ are more stable and can be transported by atmospheric winds. Because of this, the $NO_X$ enhancement can be observed after the event and far from the production area. Different secondary products can be created in such a nuclear collision; they can be further transformed by gas phase chemistry influencing the ozone balance for the ozone layer. The auroral electrons represent one of the main sources of nitrogen oxides in the thermosphere. Thus, energetic precipitating particles can directly affect the chemical composition with implications for further changes in the atmospheric dynamics and climate. The produced quantities of ions and ionization rates are important parameters determining the electric properties of the atmosphere, as well as the formation of gas admixtures and aerosols.

### *1.3. Atmospheric effects of high-energy particle precipitation (cloudiness and ozone content)*

The influences of the GCR and SEP variations on the atmosphere were studied over years [9]. The results of the analyses proved to be ambiguous. On the one hand, it was demonstrated that the galactic cosmic rays affect the high-level cloud coverage [10], the global total cloud cover [11, 12] and low cloud coverage [13]. On the other hand, the effect of the GCR variations on the cloudiness was not confirmed under detailed analysis: correlation with GCR disappears when the cloud coverage fraction is decomposed by cloud type or height, by region (reduce for ocean basis), by latitude (patterns in the tropical zone

are better associated with the concurrent El Niño) [14, 15]; the global cloudiness increases during the past century regardless of the variations of GCR [16]; the low cloud cover correlates with the solar irradiance better and more consistently than with the cosmic ray flux [17]. The total conclusion was made that the direct connection between GCR and the clouds is not evident, however, a mechanism connecting EPP ionization with clouds coverage can not be ruled out [18].

Ionization of the thermosphere and mesosphere is directly related to the formation of the ozone depleting atmospheric components. Ionization of the atmosphere controls the global electric circuit [19], which can affect the clouds properties (see, for example, [20, 21]. The GCR and SCR ionization can influence clouds formation by means of ion induced nucleation [22, 23], through cyclogenesis in the atmosphere at the low and middle latitudes [24, 25] and aerosols [4, 26, 27, 28]. Results presented in [29, 30, 31] demonstrate that the ionization rate increasing in the polar stratosphere leads to the production of aerosol nuclei, to the growth of their size and, as a consequence, to the formation of the stratospheric clouds. According to [31], an enhancement of the ionization rate by a factor of ~ 2 in the polar region under night/cold/winter conditions can lead to formation/growing of the aerosol particles in the altitude range of 10–25 km. The ozone response to the $NO_X$ и $HO_X$ increase depends on the altitude; it can even exceed the ozone response to the solar EUV irradiation in the high latitude stratosphere. The annual mean ozone depletion is the most pronounced in the mesosphere (more than 10 %) and it is also visible in the middle stratosphere, reaching 3–4 % [32].

The solar protons with energy $E_p > 90$ MeV are related to the intensification of cyclones and the cyclogenesis intensity in the Northern Atlantic, as well as to the variations of the thermo-baric fields in the troposphere at the low and middle latitudes [33, 34]. The galactic cosmic rays with energies E ~ 20–80 MeV and ~ 2–3 GeV, which precipitate, respectively, in the regions of the climatic Arctic and Polar fronts, may be involved in the processes of cyclone and anticyclone formation and development at the extra-tropical latitudes [35]. The stratospheric polar vortex is one of the most important connecting links between the solar activity and the circulation of the lower atmosphere at the extra-tropical latitudes. As the results of [36, 37, 38] demonstrate, an intrusion of the high-energy solar protons into the polar stratosphere gives rise to the growth of ionization rates, a change in chemical composition and ozone depletion. As a result, the winter stratosphere becomes cold and the stratospheric polar vortex is strengthened.

## 2. Model computations of the cosmic rays influence on atmospheric processes

### *2.1. Empirical basis for model computations*

As was indicated above, high-energy solar particles (mainly solar protons), with an energy of several to 500 MeV, enter the Earth's stratosphere and mesosphere only in the polar regions. For the first time, a sharp decrease in the ozone content in the stratosphere was detected on-board the American Nimbus-4 satellite in the course of one of the strongest flares on the Sun (August 4, 1972). As theoretical analysis has shown, high-energy particles intrusion in the polar atmosphere produced oxides of nitrogen ($NO_X$) and hydrogen ($HO_X$), which destroy ozone in catalytic chemical cycles. Later two important steps were made with the satellite missions NASA UARS (with HALOE instrument) and European ENVISAT (with MIPAS instrument). Basing on the ENVISAT measurements of ozone and other small gas components, the international project HEPPA (High Energy

Particle Precipitation in the Atmosphere) was arranged. The project involved 10 research groups including Russian teams from the Central Aerological Observatory (CAO, Moscow) [39]. As a result, model computations were performed which demonstrated good agreement with the data of satellite measurements during the solar flare in October 2003.

### *2.2. The CHARM model*

To describe the global photochemical processes taking place in the Earth's atmosphere, the numerical Chemical Atmospheric Research Model (CHARM) was elaborated in the Laboratory of Atmospheric Chemistry and Dynamics of CAO [40]. The theoretical basis for the model and a summary of the results are presented in [4, 40, 41, 42,]. The CHARM model used the "splitting method", which makes it possible to describe independently processes of advective transport and photochemical processes. One of the most accurate methods, the Prater's method, is applied to describe the transfer processes. The corresponding velocity components were calculated using the general circulation model [43]. The method of "chemical families", which can be found in [41], was used while integrating this system with chemical kinetics equations, which belong to the so-called "rigid systems". The "rigidity" of the systems of chemical kinetics equations is manifested in this case in a large range of values of the characteristic "lifetimes" of chemical components (from fractions of a second to hundreds of years), which would require very small time steps of integration. The method of "families" makes it possible to significantly decrease the "rigidity" of the system and considerably increase the time step. The photochemical block of the model describes the interaction between the 41 chemical components involved in 127 photochemical reactions. The following chemical components were calculated in the model:

– included in the chemical "families"

$O_X = O_3 + O(^3P) + O(^1D)$;

$NO_Y = N + NO + NO_2 + NO_3 + 2N_2O_5 + HNO_3 + HO_2NO_2 + ClNO_3 + N(^2D)$;

$Cl_Y = Cl + ClO + OClO + ClOO + HOCl + HCl$;

$HO_X = H + OH + HO_2 + 2H_2O_2$;

$CH_3$, $CH_2O$, $CH_3O_2$, $CH_3O_2H$, $CH_3O$, CHO, CO;

– source gases

$CH_4$, $CO_2$, $N_2O$, $CF_2Cl_2$, $CFCl_3$, $H_2$, $Cl_4$, $Cl_2$, $CH_3Cl$, $CH_2Cl$, $O_2$ (profile fixed), $N_2$ (profile fixed), $M = O_2 + N_2$ (concentration of air molecules), $H_2O$ (global distribution fixed).

The vertical profile of the molecular oxygen in the calculations was fixed. Also, the global (two-dimensional) distribution of the water vapor, based on observations from the UARS satellite (HALOE instrument), was not changed. The time step of integrating the model varied from 100 to 500 s. The dissociation rates were recalculated after 1 h of the model time, which allowed us to correctly describe the daily course of solar radiation over a fixed point. The lower boundary of the model is at the ground level, the upper boundary is at an altitude of 88 km, the height step in the model is 2 km, the resolution in latitude is 5°, and in longitude it is 10°. The initial distributions of all minor gas species (MGS) were taken from a one-dimensional photochemical model [44]. In describing the chemistry of the troposphere, the processes of "leaching" in clouds for some components ($H_2O_2$, $HNO_3$, HCl, $HNO_4$) were taken into account in parametric form. Heterogeneous reactions on the surface of aerosol particles were not taken into account. The model demonstrated computational stability when integrated over several model years and an ozone distribution consistent with observations and those obtained from other models.

### *2.3. Solar proton forcing (event of 14 July 2000)*

Let us consider the effects of solar proton intrusion in ozone in the polar atmosphere region using the example of one of the most powerful proton flares on July 14, 2000 (Bastille Day Event). It should be noted that the SPE of July 14, 2000 occurred when the Southern and Northern polar regions were in different conditions of illumination by the Sun (polar night over the south pole and polar day over the north pole). Therefore, the difference in their chemical response is of special interest. To calculate the particle ionization rates, the data from the GOES-10 satellite in various (integral) energy channels (> 5, > 10, > 30, > 50, > 100, > 370, > 480, > 640 MeV) were used. Then the corresponding differential spectra were calculated. The field of the calculated ionization velocity at each time was localized between the geomagnetic pole and latitude 66° for each hemisphere. This field was thought to be isotropic inside the polar cap. Each pair of ions formed during the deceleration of solar protons in the atmosphere leads to the formation of 1.25 nitrogen atoms and 2.0 OH radical molecules, as well as 1.15 oxygen atoms. Figure 3 shows the model ionization rate in the northern polar region caused by this event. One can see that the maximum values of the ionization rate lie in the mesosphere.

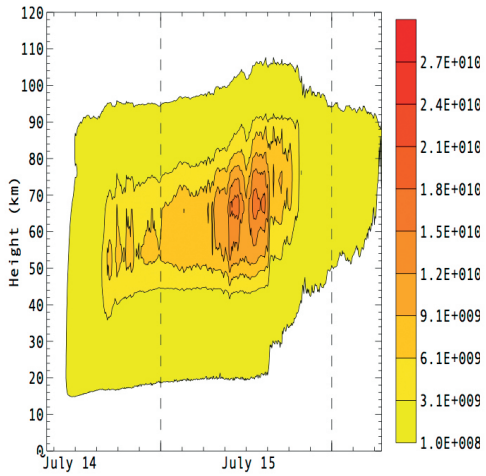


Fig. 3. Ionization produced by the solar protons in the northern polar region at latitudes from 15 to 110 km during Bastille Day Even (July 14–15, 2000); color scale on the right shows the rate of ionization, expressed as ion-pair ($m^{-3}s^{-1}$) [45]

Рис. 3. Ионизация, производимая солнечными протонами на высотах от 15 до 110 км в северной полярной области в ходе события День Бастилии (14 июля 2000 г.); цветовая шкала справа показывает уровень ионизации в единицах (ion-pair) ($m^{-3}s^{-1}$) [45]

As mentioned above, each pair of ions formed during the flash gives rise to NO and OH molecules that destroy ozone. Figure 4 (upper panel) shows the ozone destruction over the northern daylight (left) and the southern night (right) polar regions, according to model calculations [40, 46].

As the figure shows, the reaction of the ozone in the daylight and night regions is basically different. Over the daytime area, the destruction is strong (ozone in the mesosphere is completely destroyed), but ozone quickly recovers after SPE end in the presence of solar radiation (during polar day). Over the unlit area the ozone demonstrates only small depletion, without recovery.

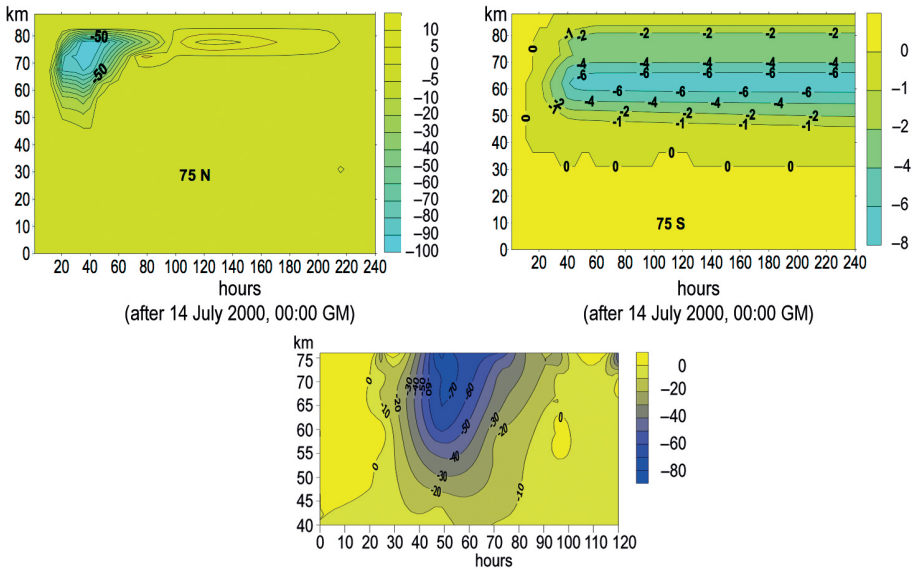


Fig. 4. Ozone changes (in %,) in the northern (left) and southern (right) polar regions caused by solar proton events on July 14, 2000: according to CHARM model (upper panel) and according to measurements on board UARS satellite (the HALOE instrument) (lower panel) [40]

Рис. 4. Изменения концентрации озона (в %) в северной (слева) и южной (справа) полярных областях в ходе события 14 июля 2000 г. согласно модельным расчетам (CHARM) (верхний ряд) и по данным измерений на спутнике UARS (прибор HALOE) (нижний ряд) [40]

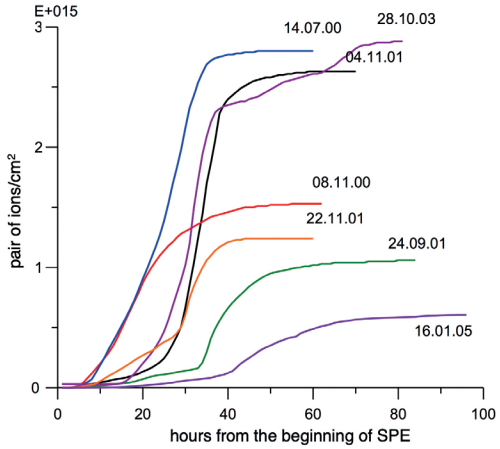


Fig. 5. Total ion production for the most powerful solar proton events (SPE) during 23th solar cycle at latitude 70° N [44]

Рис. 5. Количество ионов, образованных в столбе атмосферы на широте 70° N, во время наиболее мощных протонных событий (SPE) в 23-м цикле солнечной активности [44]

The availability of the satellite measurements covering the SPE period in July 2000 made it possible to compare the model results with experimental data. Figure 4 (lower panel) shows the results of data processing of the HALOE instrument installed on-board the American UARS (Upper Atmosphere Research Satellite) satellite, which measured ozone in the high latitudes of the northern hemisphere during the solar flare. The difference in the ozone content at 680 N between July 15, 2000 (the time of the outbreak) and July 12 (there is no outbreak yet) is shown. The experimental data and the model calculations demonstrate strong (90%) destruction of ozone in the summer mesosphere, the divergence in the scales of the graphs on the upper and lower panels should be taken into account. (Unfortunately, comparison of experimental and model results for the night polar region proved to be impossible due to a lack of experimental data). Therefore, strong solar proton events can significantly influence the ozonosphere in the sunlit polar region.

All proton events occurring in the course of the 23$^{th}$ solar cycle were analyzed in [44]. Figure 5 illustrates the total ion production for different SPE with three outstanding events, the Bastille Day Event among them. Thus, the conclusion is made that the effect of the solar particle influence should be taken into account if one is to understand correctly the variability of the polar ozone.

## 3. Ozone depletion in the Antarctic and solar UV irradiance

### *3.1. The quasi-biennial oscillation (QBO) and the 11-year solar cycle*

The quasi-biennial oscillation (QBO) is an alternation of zonal wind direction which is observed along the whole equator in a latitude belt with a half-width of ±12° in the stratosphere at pressure levels from ~100 hPa (~16 km) to ~3 hPa (~40 km). As generally accepted, the wind QBO is driven by a broad spectrum of waves, which interact with a background flow, causing a gradual alternate descent of westerly (eastward) and easterly (westward) wind regimes. The QBO is one of the main features of the general circulation in the Earth's atmosphere and the dominant source of interannual variability of large-scale dynamical processes and distribution of ozone and other trace gases not only in the tropics but also at the middle and high latitudes [47].

Apparently one of the most important effects of the QBO is the modulation of the solar influence on the Earth's atmosphere. An essential aspect of this issue is a proposed 11-year solar cycle modulation of the QBO itself [48], in particularly of the QBO period. Earlier results reported an anti-correlation of the QBO period with the solar cycle. However, later studies with a larger available data set showed instability of the correlation that can change in time [49]. However, despite the lack of a clear relationship of the QBO period with the 11-year solar cycle, a relationship of the QBO with solar activity variations at other periods cannot be ruled out. Indeed, Gruzdev et al. [50] have found a statistical link for the wind QBO and solar UV variations of the quasi-biennial time period.

### *3.2. The seasonal features and prediction of the QBO*

As the QBO is a regularly repeated feature of the atmospheric circulation, it can be useful in predicting the inter-annual variations of different phenomena on long-time scales. However, for this, a forecast of the QBO itself is required first. At present, the model predictability capacity of the QBO is limited to one-two years. Correlation scores with observational data exceed ~0.7 at a time lag of up to ~12 months, and then the level of predictability decreases [51]. This indicates that the present understanding of the QBO changes is not complete. For example, no agreement was found between the models

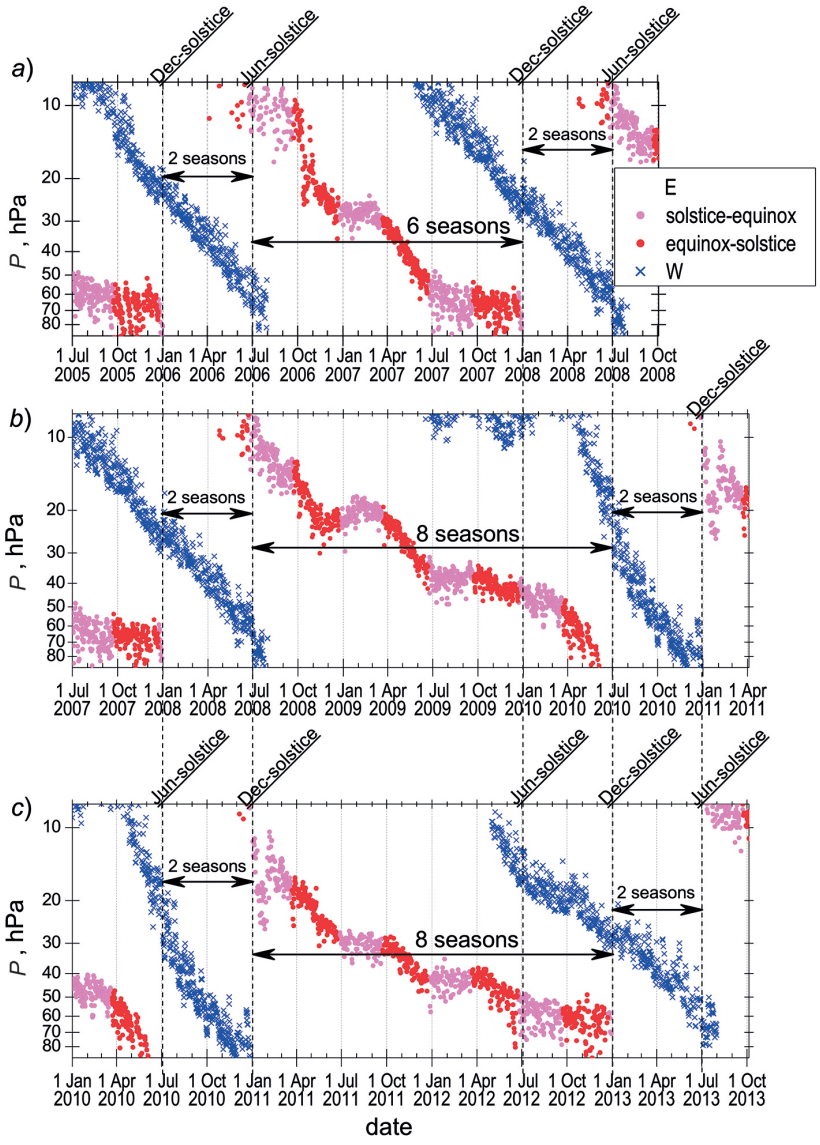


Fig. 6. Changes of the pressure level of the descending easterly wind shear derived from altitudinal profiles for the whole easterly descent from ~10 to ~70 hPa in *a*) June 2006 to December 2007; *b*) June 2008 to June 2010; *c*) December 2010 to December 2012

Рис. 6. Изменения высотного уровня (уровня давления) спускающегося сдвига восточного ветра в течение его полного спуска от ~10 до ~70 гПа, полученные по ежедневным данным о высотных профилях скорости ветра: *a*) июнь 2006 г. – декабрь 2007 г.; *b*) июнь 2008 г. – июнь 2010 г.; *c*) декабрь 2010 г. – декабрь 2012 г.

[52] in their predictions of the long-term changes of the QBO cycle period (a possible shortening or lengthening) in response to the future global warming. Apparently, this is due to differences in the representation of the basic processes driving the QBO in each model. Also, an incompleteness of the current knowledge of the QBO was demonstrated by an unexpected anomaly of the QBO in 2015–2016, which was observed after ~60 years of very regular behavior [53]. This anomaly had not been predicted by weather centers and is inexplicable in the framework of the classical commonly accepted theory of the QBO generation [47].

Seasonal dependence is an important characteristic of the QBO, which can be used for forecasting. It has been known for a very long time, but has not yet been explained. In earlier works the seasonal features were studied using monthly data of Freie Universität Berlin (hereafter FUB data) [54], and results have showed only a seasonal modulation (but not an exact synchronization) of the QBO. In our recent work [55], the descent rate of the easterly (E) and westerly (W) wind regimes was examined using daily or twice-daily observations from the Integrated Global Radiosonde Archive (IGRA) [56–57]. This study shows features that cannot be found from the monthly FUB data. Using pressure level changes of the E-wind shear, which marks the lower edge of the descending E-regime, a stepwise descent of the E-wind with alternation of intervals with a faster and slower descent rate in the full range 10–70 hPa was clearly demonstrated (Figure 6). Furthermore, the switching between different descent rates is very sharp and is observed near solstices and equinoxes. The easterly wind descends faster from equinox to solstice, while from solstice to equinox the descent rate is lower and is often near zero or even negative (a stop or ascent). Also, the beginning of the easterly at ~10 hPa and its ending near ~70 hPa are related with the solstices.

The study of all the 16 descending E-shears (using all available data in the 1977–2015 time interval, i.e. before the QBO anomaly in 2015–2016) showed that only three variants of changes in time are possible, depending on the time of the initial appearance of the E-shear at ~10 hPa and the whole time of its descent to ~70 hPa. Fig. 6 shows examples for each variant, and the scheme in Fig. 7 indicates the sequencing of the seasons, which resulted from the above seasonal links of the E-shear accelerations/decelerations. Every descent lasts either 6 or 8 seasons between appropriate solstices. The 6-season descents are limited between June and December solstices, the 8-season descents may be limited between either December solstices or June solstices. Also, the interval between the end of the previous E-shear at ~70 hPa and the appearance of the next E-shear at ~10 hPa is always equal to two seasons. The appearance of the W-shear at ~10 hPa is always observed one-to-three seasons before the end of the E-shear descent at ~70 hPa (Figures 6 and 7). But the W-shear, irrespective of the time of its appearance at ~10 hPa, always completes its descent near ~70 hPa simultaneously with the appearance of the next E-shear at ~10 hPa, and this occurs near the solstice in June or December.

Consequently, seasonal alignment of the QBO seems to be primarily associated with the seasonal regularities of the E-regime descent. The sharp changes of the descent rate of the E-wind near equinoxes and solstices are especially evident in the layer 20–50 hPa, and they can be clearly determined using even the monthly FUB data. The E-wind deceleration in the layer 20–50 hPa was earlier named stagnation stage, and the determination of the QBO period as an interval between the beginnings of the successive stagnations was suggested [58]. In this case, the QBO cycle must always begin near the solstice (in

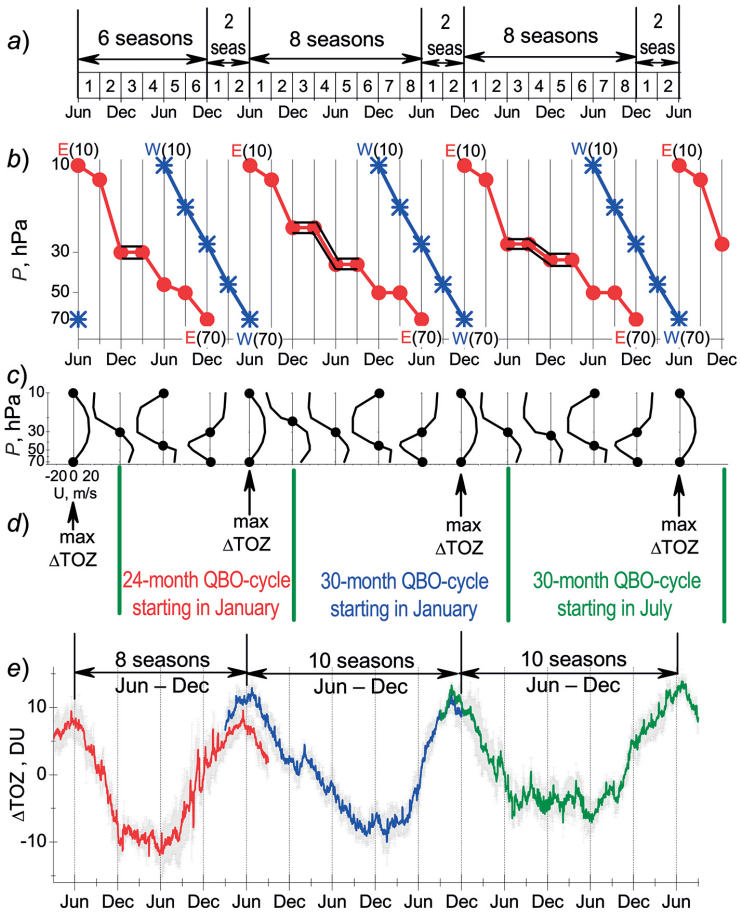


Fig. 7. The scheme for the determination of the time intervals with the identical changes of the descent of the E- and W-shear of the wind QBO, the QBO cycles and ΔTOZ changes. *a*) a sequence of the seasons; *b*) the E- (red) and W-shear (blue) descents; *c*) the height profiles of the wind speed for some months, with the big full circles at profiles indicating the levels of the wind shear; *d*) the times of the maximum ΔTOZ (the arrows below the profiles) and scenarios of the QBO cycles; *e*) the mean ΔTOZ variations at latitudes from 5°S to 5°N for three type of the QBO wind descent. The grey bars indicate the standard error of the mean.

Note that the times of the ΔTOZ maxima correspond to the end of the W-shear at 70 hPa (W70) and the simultaneous beginning of the subsequent E-shear at 10 hPa (E10)

Рис. 7. Схема определения временных интервалов с идентичными изменениями спусков E- и W-сдвига ветра КДО, циклов КДО и изменений ΔTOZ. *a*) последовательность сезонов; *b*) спуски E- (красный) и W-сдвига (синий); *c*) высотные профили скорости ветра для некоторых месяцев, большие черные кружки на профилях указывают уровни сдвига ветра; *d*) моменты максимумов ΔTOZ (стрелки под профилями) и сценарии циклов КДО; *e*) средние вариации ΔTOZ на широтах от 5° ю. ш. до 5° с. ш. для трех типов спуска ветра КДО. Серые полосы указывают стандартную ошибку среднего.

Обратите внимание, моменты максимумов ΔTOZ соответствуют окончанию спуска W-сдвига на 70 гПа (W70) и одновременному началу спуска последующего E-сдвига на 10 гПа (E10)

January or July from monthly FUB data) and its period turns out to be equal to 24, 30 or 36 months. In Fig. 7*b*, the stagnation stages are marked by black lines along the red lines for the E-shear, and Fig. 7*d* specifies possible scenarios of the QBO cycles.

Note that it is commonly believed that the QBO period varies irregularly in the range from 17 to 38 months, with the mean value being about 28–30 months. However, the discretely varying period of the QBO cycle, resulting from the seasonal regularities of the E-regime descent, allows long-term QBO prediction [59–61]. The duration of the forecasting depends on the scenario of the QBO. For example, at the beginning of the 24-month scenario of the QBO cycle the prediction is possible for the next 2 years, but at the beginning in January of the 30-month scenario the prediction is possible for the subsequent five years interval because the 30-month QBO cycle with the beginning in January is always followed by a 30-month QBO cycle with the beginning in July.

### *3.3. The dependence of the QBO on the solar UV irradiance*

The coupling of the easterly descent with seasons indicates that the equinoxes and solstices are key moments for a sharp change in the rate of the easterly descent. As is well known, the solar UV radiation, due to the absorption by ozone, affects the ozone and temperature fields in the equatorial stratosphere, but apparently the changes from solstice to equinox must be opposite to that from equinox to solstice. Thus, the seasonal variations of solar UV can cause an abrupt acceleration/deceleration of the easterly descent near equinoxes/solstices. Furthermore, the changes of the solar activity, and, correspondingly, the solar UV, at time scales of the QBO cycle period can be a source of a variety of scenarios of the QBO cycles, depending on the duration of the E-shear descent (Figs. 7*b* and 7*d*). The difference between the 6- and 8-season descents of the E-shear, which start both at ~10 hPa near the June solstice (Figs. 6a and 6*b*), is caused by various descent rates. In all the cases observed in 1977–2015, the height of the E-shear two seasons after the beginning of the E-descent (near the December solstice) was higher in the 8-season descents as compared with the 6-season. Moreover, from the December solstice to the March equinox, the ascent of the E-shear zone was observed in all the 8-season descents (as in Fig. 6*b*) [55].

A study of the solar UV in the course of the E-descents of a different duration was carried out using the Bremen Mg II composite index [62, 63], which is commonly used as a proxy for the solar UV irradiance. The long-term and short-term variations were removed from the original time series of the Mg II index by calculating a deviation of the 55-day running mean from the 360-day running mean. The resulted normalized ΔMgII index was used to determine the average UV changes coupling with the E-shear of the different descent rate and, correspondingly, the different duration.

Figure 8 shows the ΔMgII in the first year of the E-shear descents from 10 hPa to ~30 hPa. The main differences between 6- and 8-season descents, mentioned above, are apparently observed under opposite changes of the ΔMgII. Since the solar irradiance decreases (increases) from equinox to solstice (from solstice to equinox), a faster (slower) descent of the E-shear is observed under the condition of the decrease (increase) in the UV irradiance. Therefore, the additional increase in the UV irradiance due to the solar activity variations (blue line for the 8-season descent) decelerates the fast descent in the interval from equinox to solstice and changes the slow descent to ascent in the interval from solstice to equinox. And vice versa, the additional decrease in the UV irradiance due to variations of the solar activity (red line in Figure 8 for the 6-season descent) accelerates E-shear descent and therefore lowers the pressure level of the E-shear compared to the

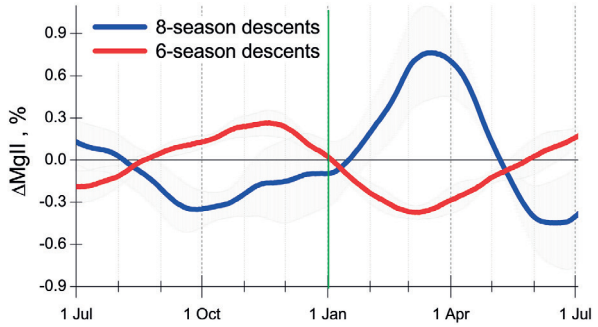


Fig. 8. Variations of the solar UV (ΔMgII index) in the course of the first year of the E-shear descents from 10 hPa to ~30 hPa. Red and blue lines are for 6- and 8-season E-descents, respectively

Рис. 8. Вариации солнечного УФ-излучения (индекса ΔMgII) в течение первого года спуска Е-сдвига от 10 гПа до ~30 гПа. Красные и синие линии показывают 6- и 8-сезонные спуски Е-сдвига соответственно

level in the 8-season descent. Hence the solar seasonal UV variations may be responsible for the stepwise E-descent with a sharp acceleration/deceleration near equinox/solstice, while the solar UV variations due to solar activity changes may cause the differences in total duration of the E-wind descent, and, accordingly, in the type of scenario of the QBO cycle (24- or 30-month scenario). A complete explanation of this relationship will require modeling experiments and comparison with observations.

### *3.4. Forecast of spring ozone depletion (ozone hole) in the Antarctic*

The quasi-biennial oscillation of the total ozone (TOZ) over the tropics is produced due to the vertical transport of ozone by a secondary meridional circulation induced by the QBO of the zonal wind. The descent of the W-shear (E-shear) is accompanied by the downward (upward) motion of air masses, and, as a result, by a growth (decrease) in the TOZ [47]. A detailed analysis of the satellite daily deseasonalized TOZ (ΔTOZ) data over the course of 15 complete wind QBO cycles, using the above mentioned seasonal features of the wind QBO, convincingly showed some new important seasonal properties of the equatorial ozone QBO [64]. Maxima of the ΔTOZ variations (Fig. 7*e*) are definitely observed near the solstice months (June or December), which are linked with time moments when the W-regime reaches ~70 hPa and the E-regime appears at ~10 hPa, which occur at the same time (Fig. 7*b*). This relation leads to the recurrence of the ΔTOZ maxima every 2 or 2.5 years. The red, blue and green lines in Fig. 7*e* depict the ΔTOZ variations that are associated with the E-shear descents of different duration: the 6-season descent, and 8-season descents beginning near June and near December solstices, respectively. But the times of the minima of the ΔTOZ are less obvious due to the W-wind appearance at ~10 hPa under the condition of the unfinished descent of the E-wind. The coupling of the wind QBO with the TOZ indicates the possibility of forecasting the equatorial TOZ variations based on the predicted wind QBO [64]. Similarly, forecasting other various processes/parameters, for which the dependence on the QBO is identified, is possible, based on the long-term forecast of the wind QBO.

For example, it is very important to predict the intensity of spring ozone depletion (ozone hole) in the Antarctic. The ozone hole is observed annually, however it is characterized by strong year-to-year fluctuations of some characteristic, such as the TOZ decrease, ozone hole area, polar vortex power, ozone mass deficit and others. The ozone

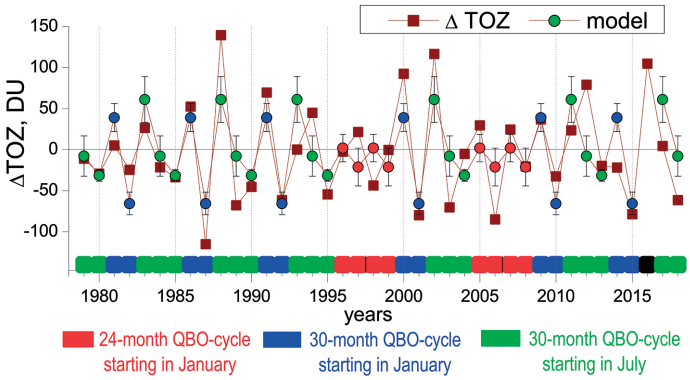


Fig. 9. Comparison of the model and actually observed fluctuations of the ΔTOZ in November in the south polar region (70–80)° S in 1979–2018

Рис. 9. Сравнение модельных и фактически наблюдавшихся вариаций ΔTOZ в ноябре в южной полярной области 70–80° ю. ш. в 1979–2018 гг.

hole is formed due to the complex influence of photochemical and dynamical processes. The increased concentration of ozone-depleting substances in the atmosphere causes a long-term negative trend in the TOZ. But year-to-year fluctuations are coupled with dynamic processes and, hence, are modulated by the QBO [47]. Therefore, the year-to-year fluctuations prevent the determination of the trend direction in recent years, and their forecast allows the identification of the natural causes of variations and the assessment of the trend due to anthropogenic factors. The forecast of ozone hole fluctuations, for example the TOZ, is based on an empirical model of the interannual fluctuations for the QBO cycles of different scenarios. The model is the average ΔTOZ variation for each type of the QBO scenario, and it is determined from experimental data over a long time interval. On the basis of the model obtained, having a long-term forecast of the QBO one can predict the ΔTOZ changes for the same period. Figure 9 shows a comparison of the model and actually observed fluctuations of the ΔTOZ in 1979–2018.

## 4. Influence of the geoeffective solar wind on atmospheric processes

### *4.1. Distinctive features of the atmospheric circulation in the Antarctic*

Katabatic winds are an exceptional feature of the atmospheric circulation in the Antarctic. The katabatic wind regime (Figure 10*a*) is a powerful drainage stream of near-surface air masses flowing from the ice dome (where the stations Vostok and Dome C are located) to the coastline [65]. This drainage is caused by negative air buoyancy supported by severe radiation cooling of the atmosphere on the ice sheet surface (due to long-wavelength radiation). The spatial structure of katabatic winds is one of the most stable atmospheric phenomena on the Earth [66]. The Coriolis force (determined by the Earth's rotation) deflects the descending air masses in the west direction, as a result the circumpolar vortex is formed at the coast line.

The powerful drainage stream permanently generates the deficiency of air masses at the Antarctic ice dome. This deficiency is compensated at the expense of air masses coming to the near-surface layer from the troposphere. As a result, a large-scale system of the vertical (meridional) circulation is formed above Antarctica [67]. The system of the vertical circulation (Figure 10*b*) includes a drainage of the air masses along the slope of

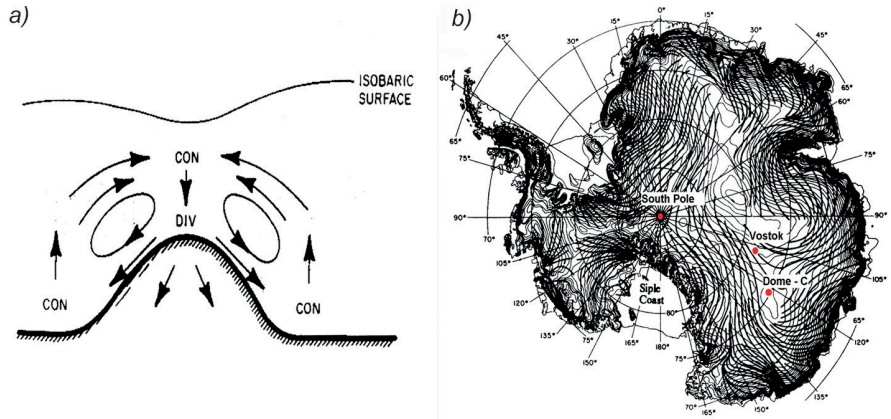


Fig. 10. The katabatic wind regime in Antarctica: *a*) conceptual scheme of the vertical mass circulation forced by katabatic winds [67]; *b*) drainage pattern of near-surface katabatic winds, red points mark the location of the inner-continental staions Vostok, Dome C and South Pole

Рис. 10. Система катабатических ветров в Антарктике: *a*) концептуальная схема циркуляции воздушных масс над Антарктикой [67]; *b*) схема распределения катабатических ветров (изолинии давления) в приземном слое Антарктики, красными точками отмечено положение станций Восток, Купол С и Южный Полюс

the ice sheet, an ascending flow near the coast line, a return movement in the lower and middle troposphere, and a descending flow above the tops of the ice dome [67, 68]. The air mass coming from the troposphere to the near-surface layer gets warm adiabatically, whereas the air mass situated on the ice sheet is subjected to a constant radiation cooling (as a result of the long wavelength radiation). These processes maintain the thermal equilibrium in the winter atmosphere. Propagation of the katabatic winds from the Antarctic ice dome is a phenomenon that involves the entire southern hemisphere [69].

### *4.2. Solar Wind influence on the atmospheric processes in the winter Antarctic*

Initially the cloudiness above the Antarctic ice dome was associated with the Forbush decrease of galactic cosmic rays during disturbed periods [10, 12]. However, a study of the cloudiness above the station Vostok (Antarctica) in the absence of Forbush decreases in the years of the solar minimum (1974–1977 and 1985–1987) showed that the cloudiness alterations were associated with the interplanetary magnetic field (IMF) Bz component [70]. The behaviour of cloudiness was examined by the data of radiation balance measurements and visual man-made observations in relation to all negative ($\Delta B_Z < -1$nT) and all positive ($\Delta B_Z > 1$nT) daily IMF $B_Z$ deviations. The rise of negative $B_Z$ was followed by the cloudiness growth and by the appropriate warming at the ground layer (altitude 3.45 km above sea level at Vostok), whereas the rise of positive $B_Z$ was followed by the cloudiness decays and the appropriate cooling. The maximum effect is observed in the day of negative Bz deviation or on the next day: the temperature at the ground level (lower panel) increased according to the cloudiness growth. It means that the cloudiness above Vostok is related to the IMF sign and, therefore, to the solar wind electric field affecting the magnetosphere

$$E_{KL} = V_{SW} \cdot (B_Y^2 + B_Z^2)^{1/2} \sin^2(\Theta/2) \text{ [71]},$$

where $V_{SW}$ is the velocity of the solar wind, $B_Z$ and $B_Y$ are the IMF components, and $\Theta$ is the angle between the IMF transverse component and the geomagnetic dipole.

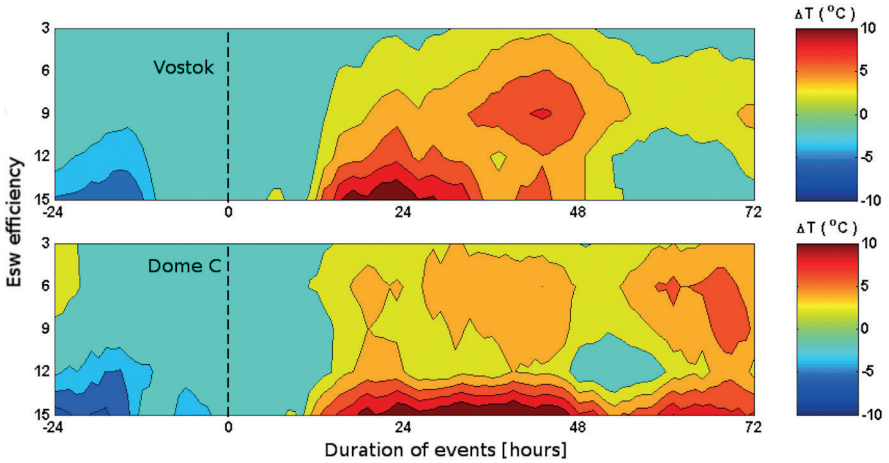


Fig. 11. Summary plot of the temperature changes ΔT at the stations Vostok and Dome C as a function of the $E_{KL}$ efficiency (left scale) [72]

Рис. 11. Диаграмма, показывающая временной ход роста температуры ΔT (правая шкала) на станциях Восток и Купол С в зависимости от величины поля $E_{KL}$ (левая шкала) [72]

Sudden warmings are another extraordinary phenomenon sometimes observed in the winter season in Central Antarctica, when the temperature on the ground level increases up to 10–15°C over some hours. As analysis [72] showed, these sudden warmings are also related to a strong increase in the solar wind electric field $E_{KL}$. Figure 11 shows a summary plot of the temperature changes ΔT (°C) at the stations Vostok (upper panel) and Dome C (lower panel) as a function of the $E_{KL}$ value (left scale) over 72 hours after the $E_{KL}$ maximum moment ($T_0$), which is marked by the dash vertical line. Red color density indicates the warming rate. The warming at the Vostok and Dome C stations starts when the interplanetary magnetic field (IMF) is southward for a long time (> 12 hours) and the solar wind electric field $E_{KL}$ effect steadily grows. The longer the electric field exposure (and the higher electric field intensity), the greater is the temperature deviation and the shorter is time delay between the key moment and the temperature change. Thus, the long influence of the intense electric field ($E_{KL}$ > 10mV/m) on the Earth's magnetosphere results in the cloud formation and the sudden warming at the stations Vostok and Dome C, located at the top of the Antarctic ice dome. As this takes place, the station South Pole, located outside of the ice dome top (see Figure 10*a*), does not display these changes.

Figure 12 demonstrates the response of the temperature (left) and atmospheric pressure (right) above the Vostok station ($h$ = 3.5–20 km) to variations of the solar wind electric field (taken in the form $E_{SW} = V_{SW} \cdot (-B_Z)$) [73, 74]. The analysis was based on the data of daily aerological measurements at Vostok in 1978–1992, the day with a maximum $E_{SW}$ deviation (*a*) or a minimum $E_{SW}$ deviation (*b*) was taken as a zero day, the temperature (or pressure) profile for the 1st day preceding the zero day being taken as the level of reference for all the succeeding days. In the case of the negative electric field leap ($\Delta E_{SW} < 0$), the atmosphere in the ground layer ($h$ = 3.45–3.5 km) gets warm within 1–2 days, but the atmosphere at altitudes of more than 10 km becomes cool. In the case of the positive electric field leap ($\Delta E_{SW} > 0$), the atmosphere in the ground layer ($h$ = 3.45–3.5 km) becomes cool, but the atmosphere at $h$ > 10 km gets warm. It implies

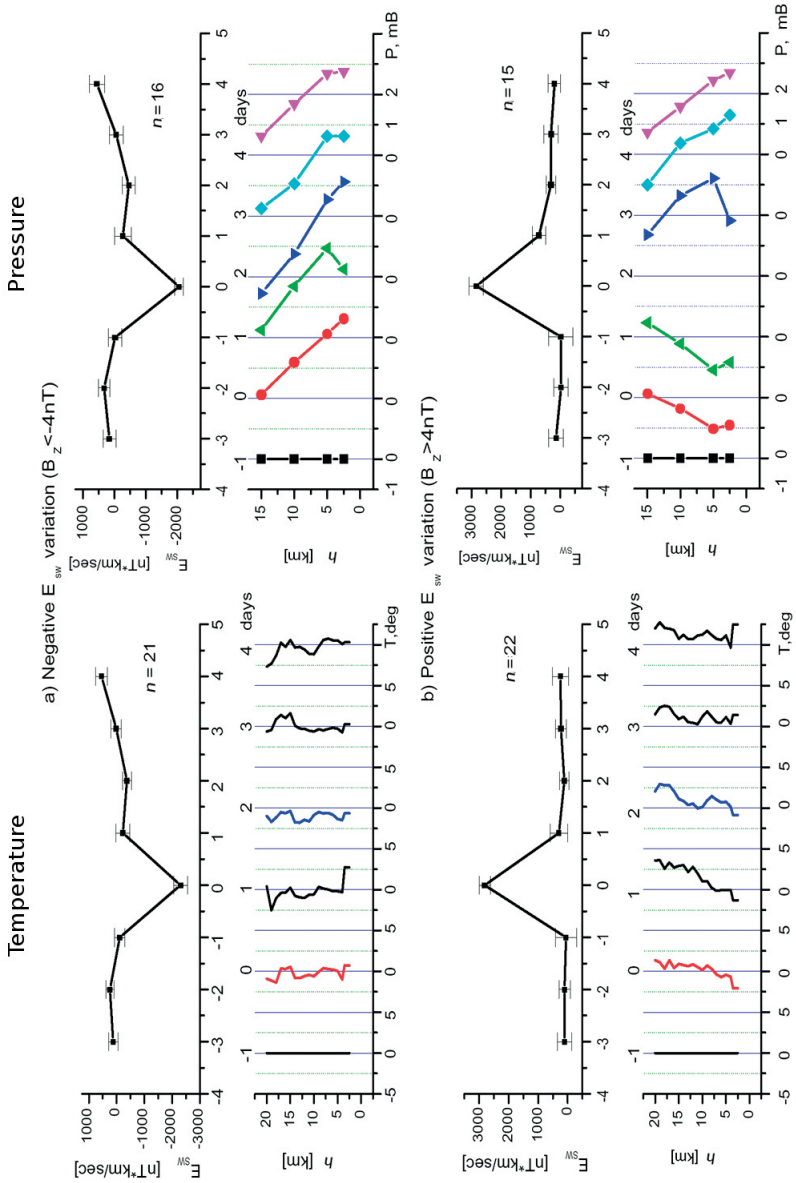


Fig. 12. Height profiles of the temperature (T) deviations and atmospheric pressure (P) deviations above the Vostok station under conditions of the negative (*a*) and positive (*b*) Esw field [73, 74]

Рис. 12. Эффект воздействия отрицательного (*a*) и положительного (*b*) межпланетного электрического поля Esw на распределение температуры T (левая колонка) и атмосферного давления P (правая колонка) на высотах от 3 до 20 км над станцией Восток [73, 74]

that the temperature at altitudes $h$ = 5–10 km remains invariant under the influence of the varying electric field. The atmospheric pressure above Vostok ($h$ = 3.5–15 km) also responds in the manner opposite to the negative and positive Esw deviations: the negative leap in $E_{SW}$ is followed by an increase in the atmospheric pressure, the positive leap in $E_{SW}$ is followed by a decrease in the atmosphere pressure in the 1st and 2nd days.

The conclusion made in [75, 76, 77] is that these phenomena are related to the vertical atmospheric circulation acting in the Antarctic in the winter season (see Figure 10). The air masses coming to the near-surface atmosphere from the troposphere, get warm adiabatically, whereas the air masses situated on the ice sheet are subjected to the constant radiation cooling due to the long wavelength radiation. These two processes maintain a thermal quasi-equilibrium in the winter atmosphere. A cloud layer is an efficient backscatter for the long-wavelength radiation going upward from the ice sheet, but it does not affect the air masses coming from above and their adiabatic warming. The reduction of the radiative cooling (because of the cloud layer) should result in a warming of the atmosphere below the cloud layer and a cooling of the atmosphere above the layer. The experimental data indicate an acceleration of the descending air masses at $h$ = 5 – 12 km in response to the negative $\Delta E_{SW}$ leap [74]. As aerological measurements above the Vostok station demonstrate, this acceleration is followed by an atmospheric pressure increase at $h$ < 10 km. The increase in the pressure above the ice dome top will strengthen the katabatic winds flowing along the ice sheet slope to the coastline.

If the descending air masses velocity exceeds the crucial level, the Coriolis force is unable to provide the westward deflection of katabatic winds. As a result, the circumpolar vortex decays and the “regular” easterlies, typical of the coast stations during the winter season, are replaced by “anomalous” southerlies. Figure 13 shows directions of the regular and “anomalous” winds above Antarctica. The regular winds at the Vostok station are winds with a low speed ($V$ < 6 m/s); the anomalous winds are winds with a higher speed ($V$ > 6 m/s). The regular katabatic winds at the coast stations are winds with azimuths in the range of 60–120°, whereas the winds with azimuths near 180° are regarded as

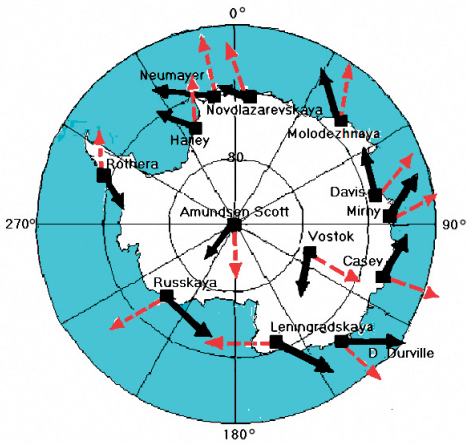


Fig. 13. Regular (black) and anomalous (red) winds in the winter Antarctica [70]

Рис. 13. Распределение регулярных (черные стрелки) и аномальных (красные стрелки) ветров в Антарктике [70]

anomalous winds. The regular winds (marked by black arrows) at the Antarctic coast form the circumpolar vortex, which is strongly related to the katabatic wind velocity [78]. The anomalous winds (red arrows) blow away from the Antarctic coast toward the equator. The relationship of the anomalous winds in the winter Antarctic to the IMF $B_Z$ component was examined in [70]. It was found that the anomalous winds are preceded for 1–2 days by a rise in the southward IMF $B_Z$ amplitude. Not all anomalous winds seen at Vostok are simultaneously observed at the coast stations: only when the strong southward IMF ($B_Z \leq -3$ nT) lasts for more 3 days do the anomalous winds spread over the entire Antarctica, and the cold Antarctic air masses rush into the Southern Ocean.

### *4.3. Mechanisms of the solar wind impact on the atmospheric processes*

The solar wind containing the southward $B_Z$ IMF component has a pronounced effect on the magnetosphere by means of the electric field $E_{KL}$ and the corresponding magnetospheric field-aligned currents (R1 FAC system). These currents, flowing into the polar ionosphere at the dawn side and flowing out of the ionosphere at the dusk side, produce the dawn-dusk voltage across the polar cap. This linkage is principally ascertained and the quantitative relationship between the electric field $E_{KL}$ and the polar cap voltage is well defined (see [71]). On the other hand, tropical thunderstorms provide a constant potential difference ~ 250 kV between the ionosphere and the Earth's surface. This potential difference ensures the downward vertical return currents, which are the most intense and variable in the polar areas (1–4 pA/m$^2$) owing to the effects of the cosmic and magnetospheric energetic particles [79, 80]. This is the way the global electric circuit is realized. Actual changes of the atmospheric electric field observed at the Vostok station represent the combination of the daily course of the tropic thunderstorms (so-called Carnegie curve) and deviations affected by the solar wind electric field [81]. The influence of the solar wind on the global electric circuit is well documented [24], but the mechanisms of the influence of the global electric circuit on the cloud formation and acceleration processes are not understood yet .

Strong increase in the southward ($B_{ZS}$) IMF component (and the corresponding increase in the geoeffective interplanetary electric field $E_{KL}$) brings into action two processes in the winter atmosphere of the Antarctic. The first is the formation of the cloud layer above the tops of the ice dome, where the air masses descend from the troposphere to the near-surface layer in the central Antarctic. As a result of the radiative cooling reduction, the atmosphere gets warm below the cloud layer and gets cool above the layer. The latter is an acceleration of the air masses coming into the central Antarctic from the troposphere. This process causes a sharp increase in the atmospheric pressure in the surface layer and gives rise to a reconstruction of the wind system above the Antarctic and a collapse of the circumpolar vortex at the periphery of the Antarctic continent. Propagation of the katabatic winds from Antarctica is a phenomenon that involves the entire southern hemisphere [69]. Thus, a significant rise of the solar wind electric field $E_{KL}$ has a crucial influence on the atmospheric processes in the winter Antarctic and Southern Ocean, and affects the formation of El-Niño and other related phenomena.

### *4.4. Influence of the Antarctic anomalous winds on Southern oscillation (El Niño and La Nina)*

ENSO is a cycle of climatic changes taking place in the tropical Pacific Ocean with a periodicity of three to seven years, with the mechanism of the changes remaining unsolved. Stable links between the Southern Oscillation and atmospheric processes in

Antarctica were found in many studies [69, 73. 74, 82, 83]. It was shown [75] that the anomalous winds (with azimuth ~190°) appear at the Antarctic coast in the 1–2 months preceding the El-Niño onset under the conditions of high magnetic activity (associated with the southward IMF). Moreover, a seasonal regularity in the occurrence of the ENSO events was revealed: the El-Niño events, associated with long-lived negative SOI deviations (> 3 months) were formed during the winter Antarctic seasons. Basing on these experimental results, a hypothesis was put forward [75, 77] that the cold anomalous winds forming in the winter Antarctic and blowing away from the Antarctic coast toward the equator will strongly impact on the Antarctic Circumpolar Current pattern acting in the Southern Ocean under usual conditions. As a result, the warm stream originating in the Western Subtropical South Pacific (WSSP ) area will be deflected from the usual south-east direction toward the equator resulting in the El Niño formation.

## CONCLUSIONS

The analysis of relationships between space weather agents and atmosphere constituents brings us to the following conclusions:

– Changes in the lower stratosphere circulation affect the surface climate.

– Galactic cosmic rays are not the main factor controlling the planetary cloudiness.

– Intense solar proton events have a strong impact on the photo-chemical processes in the polar areas and, correspondingly, on the atmospheric processes in the high-latitude regions.

– Variations of the solar UV irradiance modulate the descent rate of the zonal wind regimes in the equatorial stratosphere in the course of the quasi-biennial oscillation (QBO), and, therefore, control the total duration (period) of the QBO cycle and, correspondingly, the seasonal ozone depletion in the Antarctic.

– As a result of a drastic warming of the winter atmosphere above the Antarctic ice dome, the geoeffective solar wind impacts on the atmospheric wind system in the entire Southern Polar region, and thereby influences the dynamics of the Southern Oscillation (ENSO) and other planetary atmospheric systems.

Thus, our experimental data show a strong influence of the space weather agents and, correspondingly, solar activity on the Earth's atmosphere and, consequently, on the Earth's weather. This raises a question: does solar activity determine the Earth's climate? The solar activity in the past can be estimated by the sun spots number (SSN), which is closely related to such solar activity phenomena as solar flares and coronal mass ejections, responsible for solar influence on the Earth's atmosphere. Figure 14 (upper panel) shows SSN variations according to the data of sunspot observations, which started in the late 16th century. One can see an obvious 11-year cycle and the less pronounced ~100-year periodicity in the variations of the solar activity. The deep minimum of solar activity, known as the Maunder minimum, took place in 1640–1710. Then solar activity steadily increased up to the end of the 20$^{th}$ century, afterwards it started to decrease quickly. This regularity is very likely to be a manifestation of a 400-years periodicity in the solar activity. If this is the case, then in the near future we are in for a period similar to that of the Maunder minimum. What will be the atmospheric response to these solar activity variations?

The climate history of the Earth is often reconstructed from a variety of proxies, including ice cores, tree rings, and sediments. It should be noted that reconstructions based on tree rings [84] and those based on other sources (see for example [85–87]) provide

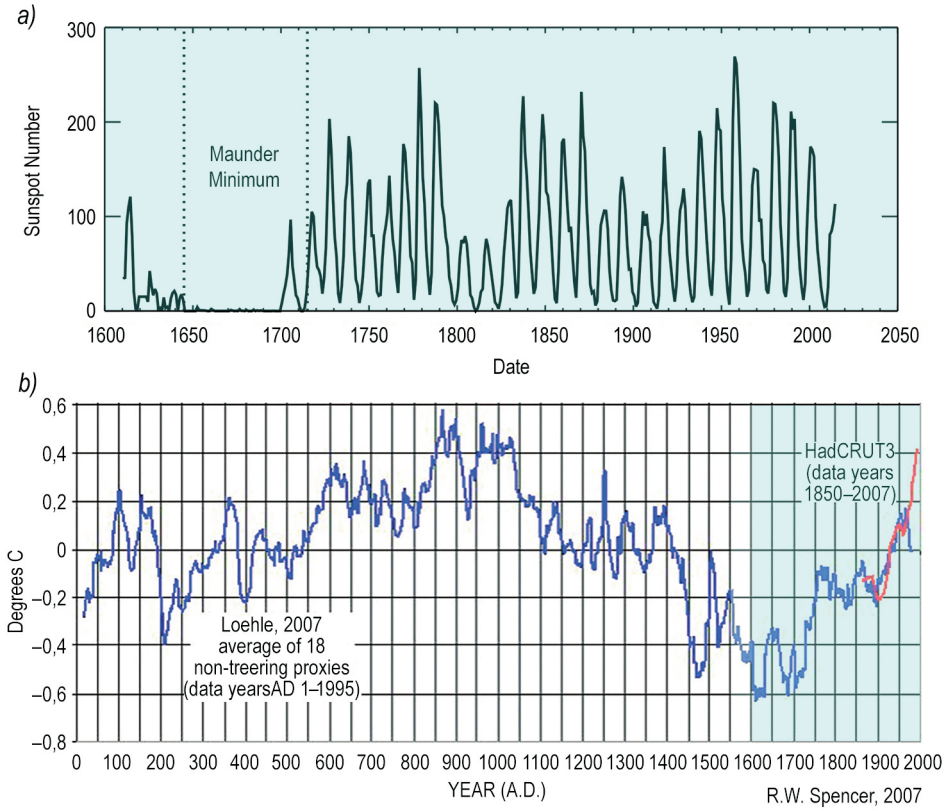


Fig. 14. Comparison of experimental data on the sun spots number (SSN) for 1600–2012 (*a*) and data on Global Temperature for 0–2000 years (*b*) [86], the blue color marks the age of the solar activity instrumental measurements

Рис. 14. Сопоставление экспериментальных данных о числе солнечных пятен (SSN) в 1600–2012 гг. (*a*) и данных о глобальной температуре Земли за последнее тысячелетие (0–2000 гг.) (*b*), голубым цветом отмечена эпоха инструментальных измерений солнечной активности

different results. Figure 14 (lower panel) shows alterations of the global temperature (the mean temperature over the Earth) for the period from 0 to 1995 [86]. One can see that the global temperature over the last 400 years strongly follows the solar activity variations: the global temperature was minimal in the 17th century, then two flat tops of temperature were observed after 1750 and around 1850, after that, during the 20th century, the Earth's temperature steadily rose. It should be noted that the highest temperatures were observed in the 9th and 10th centuries, when all technogenic emissions were non-existent and, therefore, that global warming was not associated with technogenic emissions. It means that variations of the global temperature could be due to non-anthropogenic warming, i.e. they are natural phenomena related to solar activity changes. Summing up, we have to admit that global climate changes in response to solar activity, and the latter has demonstrated the tendency to decrease in the last 15 years. If this trend proves to be steady (which will be clear in the next 5–10 years), then we will witness a global cooling (like a second Maunder minimum) instead of a global warming!

**Конфликт интересов.** Авторы заявляют об отсутствии конфликта интересов.

**Финансирование**. Работа поддержана Российским фондом фундаментальных исследований, грант N 20-15-50107.

**Вклад авторов.** Введение, заключение, разделы 1 и 4 подготовлены О.А.Трошичевым, раздел 2 написан А.А.Криволуцким, раздел 3 написан И.П.Габис.

**Благодарности.** Авторы выражают благодарность рецензентам данной статьи за полезные замечания.

**Competing interests.** The authors declare the absence of competing interests.

Funding. The work was supported by grant N 20-15-50107 from the Russian Foundation for Basic Research.

**Authors input.** The introduction, conclusions and sections 1 and 4 of this review were prepared by O.A. Troshichev, section 2 was written by A.A. Krivolutsky, section 3 was written by I.P. Gabis.

**Acknowledgements.** The authors are grateful to reviewers for fruitful remarks.

## REFERENCES

1. *Thompson D.W.J., Wallace J.M.* The Arctic Oscillation signature in the wintertime geopotential height and temperature fields. Geophys. Res. Let. 1998, 25 (9): 1297–1300.

2. *Philander S.G.H., Rasmusson E.M.* The Southern Oscillation and El Niño. Advances in Geophysics. 1985, 28A: 197–215.

3. *Bazilevskaya G., Usoskin I., Flückiger E., Harrison R., Desorgher L., Bütikofer R., Krainev M., Makhmutov V., Stozhkov Y., Svirzhevskaya A., Svirzhevsky N., Kovaltsov G.* Cosmic ray induced ion production in the atmosphere. Space Sci. Rev. 2008, 137: 149–173. doi:10.1007/s11214- 008-9339-y.

4. *Mironova I., Aplin K., Arnold F., Bazilevskaya G., Harrison R., Krivolutsy A., Nicoll K., Rozanov E., Turunen E., Usoskin I.* Energetic particle influence on the Earth's atmosphere. Space Sci. Rev. 2015, 194: 1–96. doi:10.1007/s11214-015-0185-4.

5. *Miroshnichenko L.I.* Solar cosmic rays: 75 years of research. Physics-Uspekhi. 2018, 61(4): 323–352. doi: https://doi.org/10.3367/UFNe.2017.03.038091.

6. *Mironova I., Bazilevskaya G., Kovaltsov G., Artamonov A., Rozanov E., Mishev A., Makhmutov V., Karagodin A., Golubenko K.* Spectra of high energy electron precipitation and atmospheric ionization rates retrieval from balloon measurements. Science of the Total Environment. 2019, 693: 133242. https:doi.org/10.1016/j.scitotenv.2019.07.048.

7. *Usoskin, I.G., Kovaltsov G.A., Mironova I.A.* Cosmic ray induced ionization model CRAC:CRII: An extension to the upper atmosphere. J. Geophys. Res. 2010, 115: D10302. doi:10.1029/2009JD013142.

8. *Usoskin, I.G., Kovaltsov G.A., Mironova I.A., Tylka A.J., Dietrich W.F.* Ionization effect of solar particle GLE events in low and middle atmosphere. Atmospheric Chemistry and Physics. 2011, 11 (5): 1979–1988. doi:10.5194/acp-11-1979-2011.

9. *Tinsley B.A., Brown G.M., Scherrer P.H.* Solar variability influences on weather and climate: possible connection through cosmic ray fluxes and storm intensification. J. Geophys. Res. 1989, 94: 14783–14792.

10. *Pudovkin M.I., Veretenenko S.V.* Cloudiness decreases associated with Forbush-decreases of the galactic cosmic rays. J. Atmos. Terr. Phys. 1995, 57: 1349–1355.

11. *Svensmark H., Friis-Christensen E.* Variation of cosmic ray flux and global cloud coverage — a missing link in solar climate relations. J. Solar-Terr. Phys. 1997, 59: 1225–1232.

12. *Todd M., Kniveton D.* Changes in cloud cover associated with Forbush decreases of galactic cosmic rays. J. Geophys. Res. 2001, 106: 32031–32041.

13. *Marsh N., Svensmark H.* Galactic cosmic ray and El Nino-Southern Oscillation trends in International Satellite Cloud Climatology Project D2 low-cloud properties. J. Geophys. Res. 2003, 108: 4195. doi: 10.1029/2001JD 001264.

14. *Kernthaler S., Toumi R., Haigh J.* Some doubts concerning a link between cosmic ray fluxes and global cloudiness. Geophys. Res. Let. 1999, 26 (7): 863–865. https://doi.org/10.1029/1999GL900121.

15. *Farrar P.D.* Are cosmic rays influencing ocean cloud coverage — or is it only El Nino? Climate Change. 2000, 47: 7–15.

16. *Palle E., Butler C.J.* The proposed connection between clouds and cosmic rays: cloud behavior during the past 50–120 years. J. Atmos. Solar-Terr. Phys. 2002, 64: 327–337.

17. *Kristjansson J.E., Staple A., Kristiansen J., Kaas E*. A new look at possible connection between solar activity, clouds and climate. Geophys. Res. Let. 2002, 29: 2107 doi:10.1029/2002GL015646.

18. *Harrison R.G., Carslaw K.S.* Ion-aerosol-cloud processes in the lower atmosphere. Rev. Geophys. 2003, 41: 1012–1026. doi: 10.1029/2002RG000114.

19. *Rycroft M.J., Nicoll K.A., Aplin K.L., Harrison R.G.* Recent advances in global electric circuit coupling between the space environment and the troposphere. J. Atmos. Sol.-Terr. Phys. 2012, 90–91 (1):198–211, doi:10.1016/j.jastp.2012.03.015.

20. *Tinsley B.A., Rohrbaugh R.P., Hei M., Beard K.V.* Effects of image charges on the scavenging of aerosol particles by cloud droplets and on droplet charging and possible ice nucleation processes. J. Atmos. Sci. 2000, 57: 2118–2134.

21. *Harrison R.G.* Cloud formation and the possible significance of charge for atmospheric condensation and ice nuclei. Space Sci. Rev. 2000, 94: 381–396.

22. *Marsh N., Svensmark H.* Cosmic rays, clouds, and climate. Space Sci. Rev. 2000, 94: 215–230.

23 *Carslaw K.S., Harrison R.G., Kirkby J.* Cosmic rays, clouds, and climate. Science. 2002, 298: 1732–1737. doi:10.1126/science.1076964.

24. *Tinsley B.A.* Influence of solar wind on the global electric circuit, and inferred effects on cloud microphysics, temperature, and dynamics in the troposphere. Space Sci. Rev. 2000, 94: 231–258.

25. *Mironova I., Tinsley B., Zhou L.* The links between atmospheric vorticity, radiation belt electrons, and the solar wind. Advances in Space Research. 2012, 50 (6): 783–790. doi:10.1016/j.asr.2011.03.043.

26. *Kazil J., Lovejoy E.R., Barth M.C., O'Brien K.* Aerosol nucleation over oceans and the role of galactic cosmic rays. Atmos. Chem. Phys. 2006, 6: 4905–4924.

27. *Kazil J., Harrison R.G., Lovejoy E.R.* Tropospheric new particle formation and the role of ions. Space Sci. Rev. 2008, 137: 241–255. doi:10.1007/s11214-008-9388-2.

28. *Kirkby J., Curtius J. et al*. Role of sulphuric acid, ammonia and galactic cosmic rays in atmospheric aerosol nucleation. Nature. 2011, 476 (7361): 429–433. doi:10.1038/nature10343.

29. *Mironova I.A., Desorgher L., Usoskin I.G., Fluckige E.O., Butikofer R.* Variations of aerosol optical properties during the extreme solar event in January 2005. Geophys. Res. Lett. 2008, 35: L18610. doi:10.1029/2008GL035120.

30. *Mironova I.A., Usoskin I.G.* Possible effect of extreme solar energetic particle events of September–October 1989 on polar stratospheric aerosols: a case study. Atmos. Chem. Phys. 2013, 13: 8543–8550. doi:10.5194/acp-13-8543-2013.

31. *Mironova I.A., Usoskin I.G.* Possible effect of strong solar energetic particle events on polar stratospheric aerosol: a summary of observational results. Environ. Res. Lett. 2014, 9: 015002. doi:10.1088/1748-9326/9/1/01502.

32. *Rozanov E., Calisto M., Egorova T., Peter T., Schmutz W.* Influence of the precipitating energetic particles on atmospheric chemistry and climate. Surv. Geophys. 2012, 33: 483–501.

33. *Veretenenko, S., Thejll P.* Effects of energetic solar proton events on the cyclone development in the North Atlantic. J. Atmos. Solar-Terr. Phys. 2004, 66: 393–405.

34. *Veretenenko S.V.* Comparative analysis of short-term effects of solar and galactic cosmic rays on the evolution of baric systems at middle latitudes. Bulletin of the Russian Academy of Sciences: Physics. 2017, 81 (2): 260–263.

35. *Artamonova I., Veretenenko S.* Galactic cosmic ray variation influence on baric system dynamics at middle latitudes. J. Atmos. Solar-Terr. Phys. 2011, 73 (2.3): 366–370.

36. *Veretenenko S., Ogurtsov M.* Stratospheric polar vortex as a possible reason for temporal variations of solar activity and galactic cosmic ray effects on the lower atmosphere circulation. Adv. Space Res. 2014, 54: 2467–2477.

37. *Veretenenko S., Ogurtsov M.* Cloud cover anomalies at middle latitudes: Links to troposphere dynamics and solar variability. J Atmos Solar-Terr Phys. 2016, 149: 207–218.

38. *Veretenenko S.V., Ogurtsov M.G.* Influence of solar-geophysical factors on the state of the stratospheric polar vortex. Geomagn. Aeronomy. 2020, 60: 974–981.

39. *Funke B., Baumgaertner A., Calisto M., Egorova T., Jackman C.H., Kieser J., Krivolutsky A., Lopez Puertas M., Marsh D., Reddmann T., Rozanov E., Salmi S., Sinnhuber M., Stiller G., Verronen P., Versick S., Clarmann T., Vyushkova T., Wieters N., Wissing J.* Composition changes after the "Halloween" solar proton event: the High Energy Particle Precipitation in the Atmosphere (HEPPA) model versus MIPAS data intercomparison study. Atmos. Chem. Phys. 2011, 11: 9089–9139. www.atmos-chem-phys.net/11/9089/2011/doi:10.5194/acp-11-9089-2011.

40. *Krivolutsky A.A., Vyushkova T.Yu., Cherepanova L.A., Kukoleva A.A., Repnev A I., Banin M.V.* Three-dimensional global photochemical model CHARM. Accounting for the contribution of solar activity. Geomagn. Aeronomy. 2015, 55 (1): 64–93.

41. *Krivolutsky A.A., Repnev A.I.* The impact of space factors on the Earth's ozonosphere. Moscow: GEOS, 2009: 384 p.

42. *Repnev A.I., Krivolutsky A.A.* Variations in the chemical composition of the atmosphere from satellite measurements and their relation to fluxes of energetic particles of cosmic origin. Izvestiya RAS. Atmospheric and Oceans Physics. 2010, 46 (5): 535–562.

43. *Krivolutsky A.A., Cherepanova L.A., Vyushkova T.Yu., Repnev A.I., Klyuchnikova A.V.* Global circulation of the Earth's atmosphere at altitudes of 0–135 km, calculated using the ARM model. Accounting for the contribution of solar activity. Geomagn. Aeronomy. 2015, 55 (6): 808–828.

44. *Krivolutsky A.A., Kuminov A.A., Kukoleva A.V., Repnev A.I., Pereyaslova N.K.* Proton activity of the Sun in the 23rd cycle of activity and changes in the ozonosphere: numerical modeling and analysis of observational data. Geomagn. Aeronomy. 2008, 48 (4): 450–464.

45. *Krivolutsky A.A., Klyuchnikova A.V., Zakharov G.R., Vyushkova T.Yu., Kuminov A.A*. Dynamical response of the middle atmosphere to solar proton event of July 2000: three-dimensional model simulations. Adv. Space Res. 2006, 37: 1602–1613.

46. *Ondrášková A., Krivolutsky A., Kukoleva A., Vyushkova T., Kuminov A., Zakharov G.* Response of the lower ionosphere to solar proton event on July 14 2000. Model simulations over the both poles. J. Atmos. Solar-Terr. Phys. 2008, 70: 539–545.

47. *Baldwin M.P., Gray L.J., Dunkerton T.J., Hamilton K., Haynes P.H., Randel W.J., Holton J.R., Alexander M.J., Hirota I., Horinouchi T., Jones D.B.A., Kinnersley J.S., Marquardt C., Sato K., Takahashi M.* The Quasi-biennial Oscillation. Reviews of Geophysics. 2001, 39 (2): 179–229.

48. *Salby M., Callaghan P.* Connection between the Solar Cycle and the QBO: The missing link. J. Climate. 2000, 13 (14): 2652–2663. doi: 10.1175/1520-0442(1999)012<2652: CBTSCA>2.0.CO;2.

49. *Fischer P., Tung K.K.* A reexamination of the QBO period modulation by the solar cycle. J. Geophys. Res. 2008, 113: D07114. doi:10.1029/2007JD008983.

50. *Gruzdev A.N., Bezverkhnii V.A., Schmidt H., Brasseur G.P.* Effects of solar activity variations on dynamical processes in the atmosphere: Analysis of empirical data and modeling. Turbulence, Atmosphere and Climate Dynamics. IOP Conf. Series: Earth and Environmental Science. 2019, 231: 012021. doi:10.1088/1755-1315/231/1/012021.

51. *Scaife A.A., Athanassiadou M., Andrews M., Arribas A., Baldwin M., Dunstone N., Knight J., MacLachlan C., Manzini E., Müller W., Pohlmann H., Smith D., Stockdale T.* Predictability of the Quasi-Biennial Oscillation and its northern winter teleconnection on seasonal to decadal timescales. Geophys. Res. Let. 2014, 41: 1752–1758. https://doi.org/10.1002/2013GL059160.

52. *Richter J.H., Butchart N., Kawatani Y., Bushell A., Holt L., Serva F., Kawatani Y., Bushell A.C., Holt L., Anstey J., Simpson I., Osprey S., Hamilton K., Braesicke P., Cagnazzo C., Chen C., Garcia R., Gray L., Kerzenmacher T., Lott F., McLandress C., Naoe H., Scinocca J., Stockdale T., Versick S., Watanabe S., Yoshida K.* Response of the Quasi-Biennial Oscillation to a warming climate in global climate models. Quart. Jour. Royal Meteorol. Soc. 2020. https://doi.org/10.1002/qj.3749.

53. *Osprey S.M., Butchart N., Knight J.R., Scaife A.A., Hamilton K., Anstey J.A., Schenzinger V., Zhang C.* An unexpected disruption of the atmospheric quasibiennial oscillation. Science. 2016, 353 (6306): 1424–1427. doi: 10.1126/science.aah4156.

54. The quasi-biennial-oscillation (QBO) data serie. Available at: http://www.geo.fu-berlin.de/en/met/ag/strat/produkte/qbo/index.html. (Accessed 15.01.2021).

55. *Gabis I.P.* Seasonal dependence of the quasi-biennial oscillation (QBO): New evidence from IGRA data. J. Atmos. Solar-Terr. Phys. 2018, 179: 316–336.

56. Integrated Global Radiosonde Archive (IGRA). Available at: https://www.ncdc.noaa.gov/data-access/weather-balloon/integrated-global-radiosonde-archive.(Accessed 15.01.2021)

57 *Durre I., Vose R.S., Wuertz D.B.* Overview of the integrated global radiosonde. Archive. J. of Climate. 2006, 19: 53–68.

58. *Gabis I.P., Troshichev O.A.* QBO cycle identified by changes in height profile of the zonal winds: new regularities. J. Atmos. Solar-Terr. Phys. 2005, 67: 33–44.

59. *Gabis I.P., Troshichev O.A.* The quasi-biennial oscillation in the equatorial stratosphere: seasonal regularity in zonal wind changes, discrete QBO-cycle period and prediction of QBO-cycle duration. Geomagn. Aeron. 2011, 51: 501–512.

60. *Gabis I.P.* Forecast of development of quasi-biennial oscillation in the equatorial stratospheric wind until April 2014. J. Atmos. Solar-Terr. Phys. 2012, 80: 79–91.

61. *Gabis I.P.* The validity of long-term prediction of quasi-biennial oscillation (QBO) as a proof of the exact seasonal synchronization of the equatorial stratospheric QBO cycle. J. Atmos. Solar-Terr. Phys. 2015, 124: 44–58.

62. Composite Mg II Index. Available at: http://www.iup.uni-bremen.de/UVSAT/Datasets/mgii. (Accessed 15.01.2021).

63. *Snow M., Weber M., Machol J., Viereck R., Richard E.* Comparison of Magnesium II core-to-wing ratio observations during solar minimum 23/24. J. Space Weather Space Clim. 2014, 4: A04. doi:10.1051/swsc/2014001.

64. *Gabis I.P.* Quasi-biennial oscillation of the equatorial total ozone: A seasonal dependence and forecast for 2019–2021. J. Atmos. Solar-Terr. Phys. 2020, 207 (C): 105353.

65. *Parish T.R., Bromwich D.H.* The surface windfield over the Antarctic ice sheets. Nature. 1987, 328: 51–54.

66. S*chwerdtfeger W.* Weather and Climate of the Antarctic. New York: Elsevier, 1984: 261 p.

67. *Parish T.R., Bromvich D.H.* Continental-scale simulation of the Antarctic katabatic wind regime. J. Climate. 1991, 4: 135–146.

68. *Egger J.* Slope winds and the axisymmetric circulation over Antarctica. J. Atmos. Sci. 1985, 42: 1859–1867.

69. *Bromwich D.H., Carrasco J.F., Liu Z., Tzeng R.Y.* Hemispheric atmospheric variations and oceanographic impacts associated with katabatic surges across the Ross Shelf, Antarctica. J. Geophys. Res. 1993, 98 (D7): 13045–13062.

70. *Troshichev O., Vovk V., Egorova L.* IMF associated cloudiness above near-pole station Vostok: impact on wind regime in winter Antarctica. J. Atmos. Solar-Terr. Phys. 2008, 70: 1289–1300.

71. *Troshichev O., Janzhura A.* Space weather monitoring by ground-based means: PC index. Berlin, Heidelberg: Springer Verlag, 2012: 288 p. doi:10.1007/978-3-642-16803-1.

72. *Troshichev O., Janzhura A.* Temperature alterations on the Antarctic Ice sheet initiated by the disturbed solar wind. J. Atmos. Solar-Terr. Phys. 2004, 66: 1159–1172.

73. *Troshichev O.A., Egorova L.V., Vovk V.Y.* Evidence for influence of the solar wind variations on atmospheric temperature in the southern polar region. J. Atmos. Solar-Terr. Phys. 2003, 65: 947–956.

74. *Troshichev O.A., Egorova L.V., Vovk V.Y.* Influence of the solar wind variations on atmospheric parameters in the southern polar region. Adv. Space Res. 2004, 34: 1824–1829.

75. *Troshichev O.A., Egorova L.V., Vovk V.Ya.* Influence of the disturbed solar wind on atmospheric processes in Antarctica and El-Nino Southern Oscillation. Mem. Soc. Astronomy of Italia. 2005, 76: 890–898.

76. *Troshichev O.A.* Relationship between magnetic activity in the polar cap and atmospheric processes in the winter Antarctica. J. Atmos. Solar-Terr. Phys. 2010, 72: 943–950.

77. *Troshichev O.A., Vovk V.Ya., Egorova L.V.* Solar wind influence on atmospheric processes in winter Antarctica. Antarctica: The most interactive ice-air-ocean environment. Ed. J. Singh, H.N. Dutta. Nova Sci. Publishers, 2011.

78. *Parish T.R.* On the role of Antarctic katabatic winds in forcing large-scale tropospheric motions. J. Atmos. Sci. 1992, 49: 1374–1385.

79. *Tinsley B.A., Heelis R.A.* Correlations of atmospheric dynamics with solar activity: evidence for a connection via the solar wind, atmospheric electricity, and cloud microphysics. J. Geophys. Res. 1993, 98: 10375–10384.

80. *Tinsley B.A., Zhou L.* Initial results of a global circuit model with variable stratospheric and tropospheric aerosols. J. Geophys. Res. 2006, 111, D16205: 1–23. doi: 10.1029/2005JD006988.

81. *Frank-Kamenetsky A.V., Troshichev O.A., Burns G.B., Papitashvili V.O.* Variations of the atmospheric electric field in the near-pole region related to the interplanetary magnetic field. J. Geophys. Res. 2001, 106: 179–190.

82. *Van Loon H., Shea D.J.* The Southern Oscillation, VI, Anomalies of sea level pressure on the southern hemisphere and of Pacific sea surface temperature during the development of a warm event. Mon. Weather Rev. 1987, 115: 370–379.

83. *Smith S.R., Stearns C.R.* Antarctic pressure and temperature anomalies surrounding the minimum in the Southern Oscillation Index. J Geopys. Res. 1993, 98 (D7): 13071–13083.

84. *Mann M.E., Jones P.D.* Global surface temperatures over the past two millennia. Geophys. Res. Lett. 2003, 30 (15): 1820. doi:10.1029/2003GL017814.

85. *Moberg A., Sonechkin D.M., Holmgren K., Datsenkoet N.D., Karlin W.* Highly variable Northern hemisphere temperatures reconstructed from low- and high resolution proxy data. Nature. 2005, 433 (7026): 613–617.

86. *Loehle C.* A 2000-year Global temperature reconstruction based on not-treering proxies. Energy and Environment. 2007, 18 (7): 1049–1058.

87. *Demezhko D.Y., Golovanova I.V.* Climatic changes in the Urals over the past millennium? An analysis of geothermal and meteorological data. Climate of the Past. 2007, 3 (2): 237–242.

## Влияние космической погоды на земную атмосферу (расширенный реферат)

Термином «космическая погода» называют комплекс явлений и процессов в гелиосфере, обусловленных «солнечной активностью» — непрерывным, но меняющимся во времени излучением солнечной плазмы и электромагнитных волн в космическое пространство. Основными компонентами космической погоды являются: волновое электромагнитное излучение, солнечный ветер — поток низкоэнергичной солнечной плазмы, излучаемой всей поверхностью Солнца, корональные выбросы плазмы и высокоскоростные потоки, связанные с солнечными активными областями («возмущенный солнечный ветер»), солнечные и галактические космические лучи (потоки высокоэнергичных протонов и электронов с энергией E > 500 МэВ).

Волновое (световое и тепловое) солнечное излучение определяет условия жизни на Земле, но его изменения в связи с солнечной активностью очень незначительны и приходятся в основном на УФ-область спектра, что обуславливает вариации долготно-широтного распределения озона в земной атмосфере. Энергетический вклад корпускулярной радиации пренебрежимо мал по сравнению с волновой радиацией, но она критически меняет условия прохождения волновой радиации через атмосферу и сильно варьирует, с периодичностью от суток до сотен лет в зависимости от солнечной активности. Актуальность исследования таких вариаций и их влияния на атмосферные процессы становится особенно очевидной в свете происходящих в настоящее время глобальных климатических изменений.

Космические лучи солнечного и галактического происхождения и высокоэнергичные электроны магнитосферного происхождения Земли, проникающие в земную атмосферу, ионизуют нейтральные молекулы азота и водорода, создавая химически активные окислы азота и водорода, которые разрушают атмосферный озон. В зависимости от энергии частиц, которая определяет глубину их проникновения, ионизация происходит на высотах мезосферы или стратосферы. Именно этот механизм солнечно-атмосферных связей объясняет межгодовую изменчивость содержания озона в полярных областях. Исследования, выполненные в рамках международного проекта HEPPA (High Energetic Particle Precipitation in the Atmosphere), в котором принимали участие представители 10 стран, включая Россию, позволили перейти к модельным расчетам воздействия частиц солнечного происхождения на атмосферу, основанным на экспериментальных спутниковых данных о содержании озона и других малых газовых составляющих атмосферы. В последние годы российскими учеными были созданы глобальные фотохимические модели, включающие химические реакции ионной химии, что позволяет изучить воздействие вспышек на Солнце на области D и E полярной ионосферы.

Ионы, генерируемые в атмосфере под воздействием заряженных частиц, увеличивают скорость образования ядер конденсации аэрозолей, что определяет такие климатические последствия, как формирование облачности, циклоническая активность, атмосферная циркуляция. Полученные экспериментальные данные свидетельствовали о влиянии меняющегося корпускулярного излучения на погоду и климат, на облачность в верхнем ярусе атмосферы, на температуру полярной тропосферы, на глобальную облачность и на облачность в нижнем ярусе атмосферы.

Уникальность атмосферных процессов в Антарктике, где наличие континентального ледяного купола обеспечивает стабильную систему вертикальной атмос-

ферной циркуляции, обеспечивает возможность анализа воздействия на атмосферу возмущенного солнечного ветра (длительное воздействие интенсивного межпланетного электрического поля). Показано, что воздействие реализуется через глобальную электрическую цепь и определяет режим аномальных атмосферных ветров в зимней Антарктике. С режимом аномальных атмосферных ветров связано формирование отрицательной фазы (Эль-Ниньо) в системе южной атмосферной циркуляции ENSO. Система ENSO является самой мощной планетарной системой на Земле, которая определяет не только климатический режим в Южном полушарии, но влияет и на погодные условия в Северном полушарии (системы AO и NAO).